8-31-2017

Influence of Slippery Pacemaker Leads on Lead-Induced Venous Occlusion

Sagar Bhatia
Santa Clara University, sbhatia@scu.edu

SANTA CLARA UNIVERSITY
Department of Mechanical Engineering

August 31st, 2017

I HEREBY RECOMMEND THAT THE THESIS PREPARED UNDER MY SUPERVISION BY

Sagar Bhatia

ENTITLED

Influence of Slippery Pacemaker Leads on Lead-Induced Venous Occlusion

BE ACCEPTED IN PARTIAL FULFILLMENT OF THE REQUIREMENTS FOR THE DEGREE

OF

MASTER OF SCIENCE IN MECHANICAL ENGINEERING

ON SHUN PAK, THESIS ADVISOR

DARZEN FABRIS, THESIS READER

DARZEN FABRIS, CHAIRMAN OF DEPARTMENT

INFLUENCE OF SLIPPERY PACEMAKER LEADS ON LEAD-INDUCED VENOUS OCCLUSION.

BY

SAGAR BHATIA

MASTER OF SCIENCE THESIS

SUBMITTED IN PARTIAL FULFILLMENT OF THE REQUIREMENTS
FOR THE DEGREE OF MASTER OF SCIENCE
IN MECHANICAL ENGINEERING IN THE SCHOOL OF ENGINEERING
SANTA CLARA UNIVERSITY, 2017

SANTA CLARA, CALIFORNIA, USA

Acknowledgments

I would like to express my sincere gratitude to my advisor Dr. On Shun Pak for the continuous support of my Master's thesis, for his patience and motivation throughout my research.

I would also like to thank Dr. Darzen Fabris for being the reader of this thesis.

Thanks to Dr. Herve Nganguia for his help with the eccentric cylinder derivations and Dr. Weiguang Yang for providing the patient-specific models and helping with the simulations.

Contents

List of Figures

Nomenclature

C	Focal distance in bipolar coordinate system
H	Center-to-center distance
Q	Volume flow rate
R_i	Inner cylinder radius
R_o	Outer cylinder radius
$\mathbf{u}$	Velocity vector
e	Eccentricity
l	Slip length
n	Normal direction
p	Pressure
r	Radial distance
u	Tangential velocity
u_z	z-direction velocity
w	Dimensionless velocity
β	Slip coefficient
λ	Dimensionless slip length
λ_1	Dimensionless slip length of inner cylinder

λ_2	Dimensionless slip length of outer cylinder
μ	Viscosity
τ	Wall shear stress
ξ_1	Inner cylinder surface
ξ_2	Outer cylinder surface
ω	Angular distance

ABSTRACT

The use of medical devices such as pacemakers and implantable cardiac defibrillators have become commonplace to treat arrhythmias. Pacing leads with electrodes are used to send electrical pulses to the heart to treat either abnormally slow heart rates, or abnormal rhythms. Lead induced vessel occlusion, which is commonly seen after placement of pacemaker or implantable cardiac defibrillators leads, may result in lead malfunction and/or superior vena cava syndrome, and makes lead extraction difficult. The association between the anatomic locations at risk for thrombosis and regions of venous stasis have been reported previously. The computational studies reveal obvious flow stasis in the proximity of the leads, due to the no-slip boundary condition imposed on the lead surface. With recent technologies capable of creating slippery surfaces that can repel complex fluids including blood, we explore computationally how local flow structures may be altered in the regions around the leads when the no-slip boundary condition on the lead surface is relaxed using various slip lengths. The slippery surface is modeled by a Navier slip boundary condition. Analytical studies are performed on idealized geometries, which were then used to validate numerical simulations. A patient-specific model is constructed and studied numerically to investigate the influence of the slippery surface in a more physiologically realistic environment. The findings evaluate the possibility of reducing the risk of lead-induced thrombosis and occlusion by implementing a slippery surface conditions on the leads.

Chapter 1

Introduction

A pacemaker is a small device that is placed in the chest or abdomen to help control abnormal heart rhythms. It uses low-energy electrical pulses to prompt the heart to beat at a normal rate. Pacemakers are used to treat arrhythmia, which represents any change in the normal sequence of electrical impulses. The electric impulse may happen too fast, too slow, or erratically that would result in an abnormal heart beat. The improper heart beat would cause ineffective blood flows to different parts of the body, which may lead to damages or shut down of other organs. Previous studies show that in $1-3\%$ of patients with pacemaker implants are symptomatic to occlusions right after the implantation [1]. But, the number of cases of venous occlusions increases to $14-37\%$ when the patients return for system revision or regular follow up [2–5]. From the year 1980 to 2003, the number of pacemaker implants has increased from 40,000 per year to 150,000 per year. In 2006, an estimate of 418,000 pacemakers was implanted in United States [6].

Despite the common use of these medical devices, a complete understanding of the risk factors for the development of venous obstruction and methods to circumvent them however remain to be addressed. The majority of pacemaker failure is caused by venous occlusion. Figa *et al.* [7] suggested that lead characteristics are significant factors affecting the occurrence of venous occlusion in young patients. The presence of pacemaker leads in the blood vessel may cause more occlusions in young patients because of their small blood vessels than adult patients. In some cases of pacemaker implantation, the pacemaker leads cause partial or full blockage of the blood flow in a vessel. The blockage causes increased wall shear stress on the blood vessels and

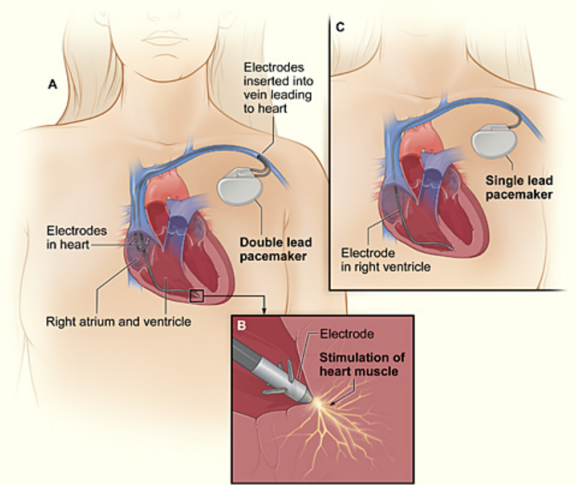

Figure 1.1: Schematic representation of a pacemaker implant. Image taken from NIH website [8] without permission.

decreased blood flow rates.

Computational fluid mechanics has been employed as a useful tool to simulate the flows of blood in both idealized and patient-specific geometries [9]. In particular, for lead-induced venous occlusion, a simulation-based investigation was conducted with patient-specific geometrical models to predict the locations of the vessels that are prone to venous occlusions [10]. Using the images obtained from computed tomography (CT) scan of patients, three-dimensional (3D) models of blood vessels were created as shown in Fig. 1.2. These models were then used to perform fluid dynamics simulations to analyze different flow characteristics, including blood flow velocity, wall shear stress, and pressure with and without the pacemaker lead.

Typically the pacemaker leads used in the implants are made of metal alloys insulated with silicone rubber or polyurethane. While studying the fluid mechanics of blood flow around such pacemaker leads, the pacemaker lead surface is considered as a no-slip surface. This results in regions with low velocities near the lead and results in an increase in the wall shear stress on the blood vessel [10]. As shown in Fig. 1.3, the flow velocity is typically low near the lead. This results in increased mean exposure time, which is the amount of time fluid particles stay in a particular region. Regions with higher mean exposure time distribution are more prone to occlusions or blockage because the blood cells have more time to interact with the lead surfaces to develop thrombosis.

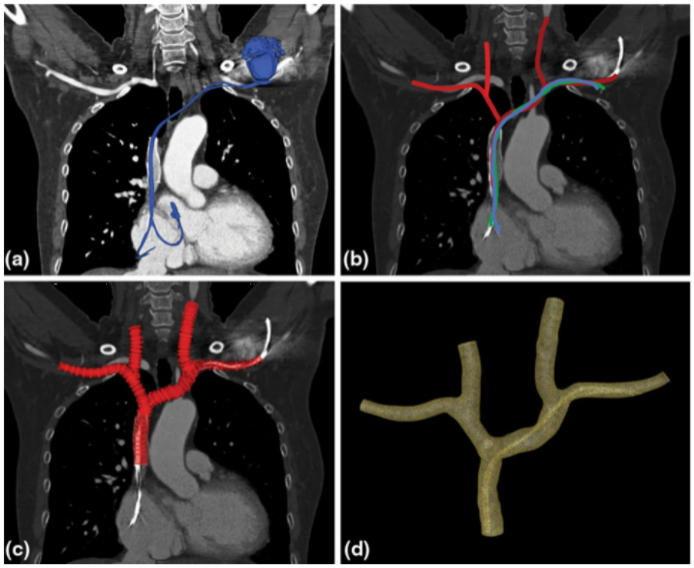

Figure 1.2: Patient-specific geometrical models. (a) Patient-specific CT image with pacemaker lead and generator highlighted. (b) Paths drawn through the center of the great vain (red) and lead (green and blue) (c) The vessel lumen is defined at fixed intervals along each vessel and these slices are lofted together to provide a geometric model of the great veins and pacemaker leads (d) High-resolution computational mesh is created from the geometric model [10]. Image reproduced from [10] without permission.

In this work, we explore the influence of surface condition of the pacemaker lead on the local flow structure by relaxing the no-slip boundary condition on the lead surface. These "slippery" surfaces may be achieved with superhydrophobic materials inspired by lotus leaves [11], which lead to the development of liquid repellent micro-textured surfaces. Recently, Wong *et al.* [12] have developed slippery liquid-infused porous surfaces (SLIPS) technology. The idea was inspired by Nepenthes pitcher plants shown in Fig. 1.4, and these SLIPS materials posses nano-structured tubes infused with lubricating fluids. The slippery surface is highly hydrophobic and stable under pressure. These SLIPS materials are biocompatible and capable of repelling biological fluids including untreated blood samples, which suggest their applications in anti-biofouling coatings for medical devices (Fig. 1.5). Some previous studies also demonstrated significant drag reduction using these slippery surface [14–17].

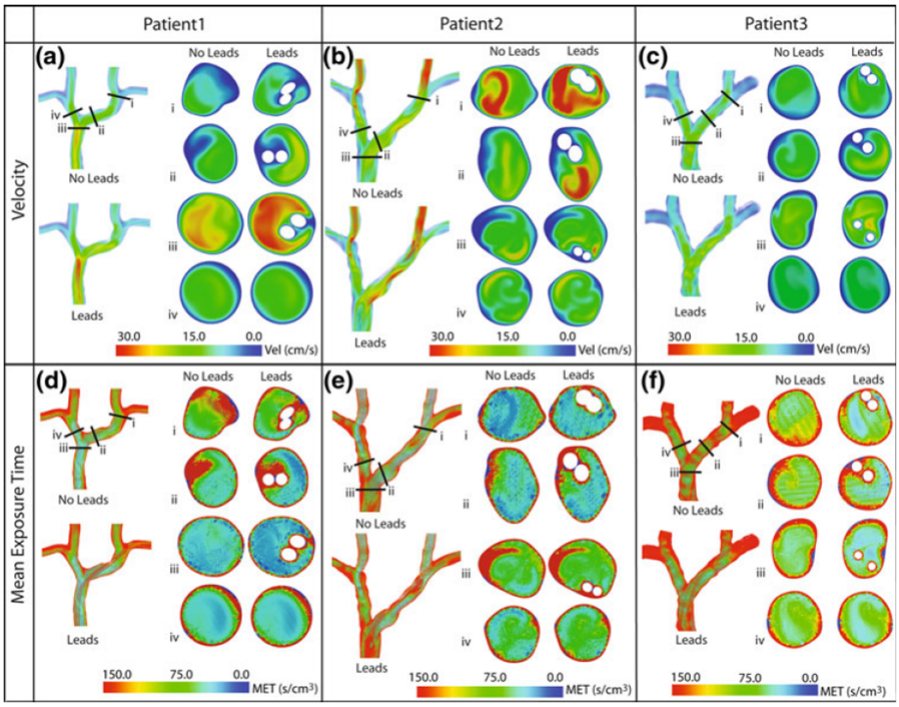

Figure 1.3: Comparison of velocity and mean exposure time distributions for different patient-specific models at various locations with and without pacemaker leads [10]. Image reproduced from [10] without permission.

For different physical reasons and scenarios, the slip flows have been noticed earlier in gas flows, non-newtonian fluids and contact line motion [18]. The influence of slippery surfaces on flow structure can be modeled through an apparent slip length described by the Navier slip condition [19] as,

$$u = l\frac{\partial u}{\partial n}, \tag{1.1}$$

where u is the tangential velocity, l is the dimensional slip length of the surface, and n is the normal direction. The slip length of surfaces produced from different technologies can range from few micrometers to hundreds of micrometers [17].

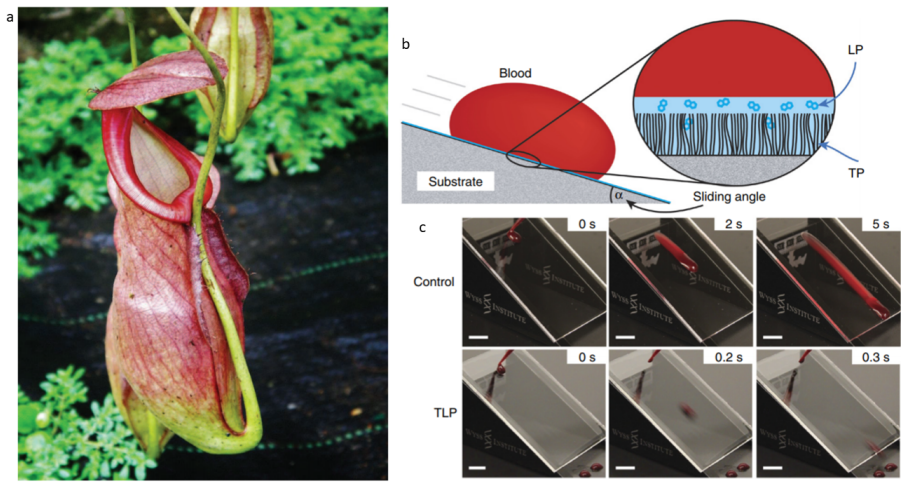

Figure 1.4: (a) Nepenthes pitcher plant (b) Microscopic view of SLIPS, LP-liquid perfluorocarbon, TP-tethered perfluorocarbon. (c) Residual on blood droplet on tethered liquid perfluorocarbon(TLP) and on acrylic [13]. Image reproduced from [13] without permission.

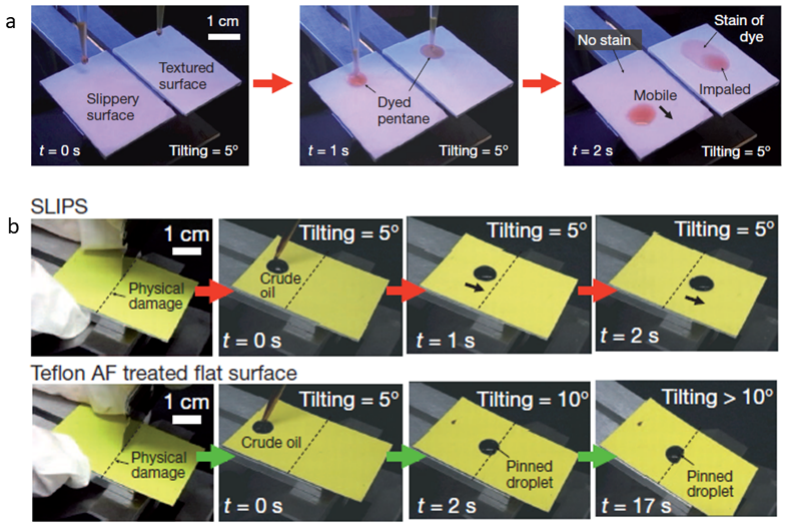

Figure 1.5: (a) Flow comparison over SLIPS and superhydrophobic, air containing Teflon porous surface. Fluid flows on SLIPS without leaving any residual but leaves some traces behind on the Teflon surface. (b) Flow over the SLIPS and Teflon surface after physical damage. Fluid flows on SLIPS over the damaged part without leaving any residual but gets pinned on the damaged part while flowing over Teflon surface [12]. Image reproduced from [12] without permission.

In this work, we investigate theoretically the influence of a slippery pacemaker lead on the flow characteristic in blood vessels. We first perform analytical studies for idealized vessel geometries in Ch. 2 to obtain some fundamental understanding of the effects of apparent slip on lead surface. The analytical results are then used to compare with the numerical results obtained from numerical simulations to validate the numerical results in Ch. 3. After validation, a 3D patient-specific model is created to investigate the effect of a slippery lead surface in more realistic biological scenarios, and the results are discussed in Ch. 3.

Chapter 2

Analytical Studies

Before considering complex geometries in patient-specific models, idealized geometries are studied here to make analytical progress. These analytical results provide basic understandings and can be used for validating the numerical simulation results later.

Poiseuille pioneered the modeling of blood flows by studying the ideal scenario of pressure-driven flow in a long circular pipe. Assuming blood as a Newtonian fluid and the flow being incompressible, the fluid velocity $\mathbf{u}$ and pressure p is governed by the continuity equation (conservation of mass):

$$\bigtriangledown \cdot \mathbf{u} = 0, \tag{2.1}$$

and the Navier-Stokes equation (conservation of momentum):

$$\rho \left[\frac{\partial \mathbf{u}}{\partial t} + \mathbf{u} \cdot \bigtriangledown \mathbf{u} \right] = - \bigtriangledown p + \mu \bigtriangledown^2 \mathbf{u}, \tag{2.2}$$

where ρ and μ represent the fluid density and dynamic viscosity, respectively. Under the assumptions of a steady and unidirectional flow in the z-direction in cylindrical polar coordinates (r, ϕ, z), the velocity field u_z satisfying the no-slip boundary condition on the wall of a blood vessel ($r = R_o$) is given by

$$u_z = \frac{1}{4\mu} \frac{\partial p}{\partial z} \left(r^2 - R_o^2 \right), \tag{2.3}$$

where $\partial p / \partial z$ is the pressure gradient. The simplest model that accounts for the presence of a pacemaker lead is that of flow past concentric cylinders. The inner cylinder represents the pacemaker lead and the outer cylinder presents the blood vessel. This problem can also be readily solved in cylindrical polar coordinates with

the no-slip boundary condition at both the inner and outer cylinders. The resulting unidirectional flow field is given by

$$u_z = \frac{1}{4\mu}\frac{\partial p}{\partial z}\left[r^2 - R_o^2 - \frac{\ln(r/R_o)}{\ln(R_o/R_i)}(R_o^2 - R_i^2)\right], \tag{2.4}$$

where R_o and R_i are the outer and inner radii respectively.

2.1 Concentric cylinders with non-homogeneous slip

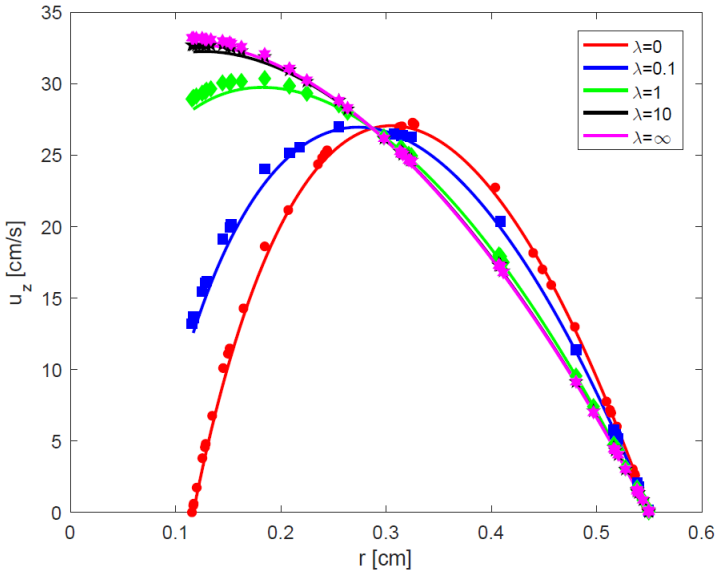

Figure 2.1: Velocity profiles in concentric cylinders for different slip lengths, λ = 0, 0.1, 1, 10 and ∞. Here λ is the dimensionless slip length on the inner cylinder surface. The solid lines represent the analytical results and the symbols represents the simulation results (see Ch. 3).

In the idealized scenario of having a pacemaker lead concentrically positioned along the centerline of a blood vessel, one can investigate the effect of a slippery surface by implementing a Navier slip boundary condition introduced in Eq. 1.1 at the inner cylinder ($r = R_i$). The boundary condition at the outer cylinder ($r = R_0$) remains to be no-slip since it represents the blood vessel. This known solution [19] is reviewed below since it will be used as a validation for subsequent numerical simulations.

We non-dimensionalize lengths by the outer radius R_0 and velocities by GR_o^2/μ, where G is the negative pressure gradient. The dimensionless Navier slip boundary

condition for the dimensionless velocity w is then given by

$$w = \lambda \frac{\partial w}{\partial n}, \tag{2.5}$$

where $\lambda = l/R_0$ is the dimensionless slip length. The dimensionless velocity expression for non-homogeneous slip at the inner and outer cylinders can be calculated as [19],

$$w = c_1 + c_2 \ln r - \frac{r^2}{4}, \tag{2.6}$$

with

$$c_1 = \frac{1}{4}\left[1 + 2\lambda_2 - \frac{b\lambda_2(1 - b^2 + 2b\lambda_1 - 2\lambda_2)}{(\lambda_1 + b\lambda_2 - b\ln b)}\right], \tag{2.7}$$

$$c_2 = \frac{b(1 - b^2 + 2b\lambda_1 + 2\lambda_2)}{4(\lambda_1 + b\lambda_2 - b\ln b)}, \tag{2.8}$$

where $b = R_i/R_o$, $\lambda_1 = l_1/R_o$ is the dimensionless slip length of inner cylinder surface and $\lambda_2 = l_2/R_o$ is the dimensionless slip length of outer cylinder surface (l_1 and l_2 are the dimensional slip length of inner and outer cylinder surface respectively). The dimensional version of the velocity field is given by

$$u_z = -\frac{\partial p}{\partial z}\frac{R_o}{\mu}\left[c_1 + c_2 \ln\left(\frac{r}{R_o}\right) - \left(\frac{r}{2R_o}\right)^2\right]. \tag{2.9}$$

Applying this general solution to the specific problem of a concentric pacemaker lead in a blood vessel, we consider a blood vessel raids of $R_o = 0.55$ cm and pacemaker lead radius as $R_i = 0.1167$ cm. We assume a viscosity of $\mu = 0.04$ g/cm.s for blood and a physiological volume flow rate $Q = 16$ cm^3/s. The outer cylinder wall is considered as no-slip surface (i.e. $\lambda_2 = 0$) and different slip length values on inner cylinder wall are considered to calculate the velocity profile as shown in Fig. 2.1. As expected, the slip velocity at the pacemaker lead ($r = R_i$) increases with the slip length, but the rate of increase is less substantial for large values of λ. A dimensionless slip length of $\lambda = 1$ already develops mores than 80% of the slip velocity generated by the free slip case $\lambda = \infty$. Therefore, even though current technologies can only produce a slippery surface with slip lengths in the order of hundreds of micrometers, their effects may still be significant in small scale flows.

Wall shear stress at the blood vessel ($r = R_0$) is an important quantity in the biomechanics of cardiovascular systems because the endothelial cells were shown to

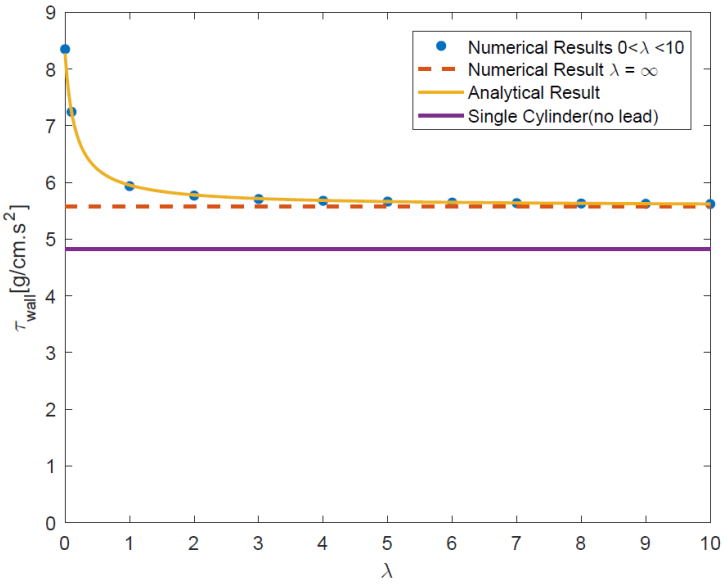

Figure 2.2: Comparison between analytical results and simulation results for wall shear stress on the blood vessel (outer cylinder), where no-slip boundary condition is applied. The slip length λ of the pacemaker lead (inner cylinder) is varied.

respond to shear stresses. The corresponding dimensional wall shear stress in the above problem is calculated as

$$\tau_{wall} = R_o \frac{\partial p}{\partial z} \left[\frac{c_2}{R_o} - \frac{1}{2R_o} \right]. \tag{2.10}$$

For this axisymmetric case, the wall shear stress is uniform and Fig. 2.2 shows the change in numerical values of the wall shear stress with the slip length (λ) on inner cylinder wall surface. The wall shear stress when there is no lead is given shown for comparison. For a pacemaker lead with no-slip boundary condition ($\lambda = 0$) is present, the wall shear stress at the blood vessel increases substantially ($\approx 70\%$). Such a substantial increase in wall shear stress might cause undesirable response of the endothelial cells. When the surface of the pacemaker lead becomes increasingly slipper (increasing λ), the wall shear stress decreases to a value closer to the case when there is no lead.

2.2 Eccentric cylinder with non-homogeneous slip

Next, we consider the case when the pacemaker lead (inner cylinder) is eccentrically positioned in side the blood vessel, which represent a more realistic scenario compared with the concentric case. Problems with eccentric cylinders can be treated analytically with the bipolar cylindrical coordinates (Fig. 2.3). The slip flow past eccentric annulus with homogenous slip boundary conditions (*i.e.* same slip length for all surfaces) have been recently solved by Alassar in a semi-analytical approach in bipolar cylindrical coordinates [24]. To adapt the calculations to our problem where the slip lengths are different on the inner (slippery pacemaker lead) and outer (no-slip good vessel) surfaces, we pursue a slight modification of the calculation by Alassar [24] to allow a simple extension of their results to non-homogenous slip boundary conditions.

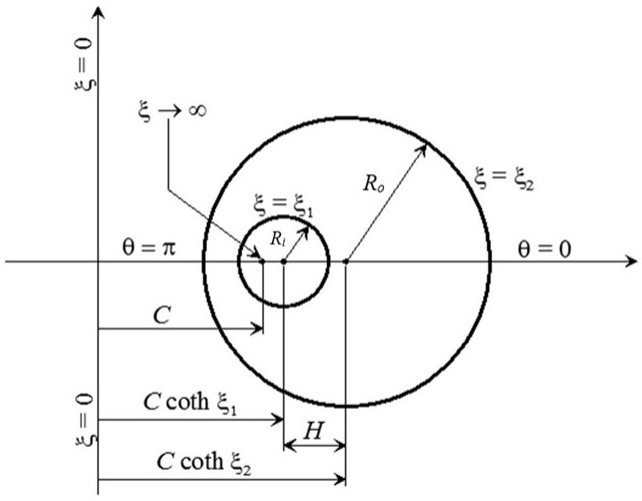

Figure 2.3: Bipolar cylindrical coordinate system, image taken from Alassar [24].

We will first reproduce the calculations by Alassar [24] in Sec. 2.2.1, before presenting new results for non-homogenous slip in Sec. 2.2.2.

2.2.1 Homogenous slip

In this section, we present the formulation by Alassar [24] on the slip flow through an eccentric cylindrical annulus and reproduce their results as a validation. The problem is solved in bipolar cylindrical coordinate system (θ, ξ, z), shown in Fig. 2.3, where there are two foci. The relation between the bipolar cylindrical coordinate and Cartesian coordinate systems is given by:

$$x = \frac{C \sinh \xi}{\cosh \xi - \cos \theta}, \tag{2.11}$$

$$y = \frac{C \sin \theta}{\cosh \xi - \cos \theta}, \tag{2.12}$$

$$z = z, \tag{2.13}$$

where C is the focal distance

$$C = \frac{\sqrt{(H - R_i - R_o)(H - R_i + R_o)(H + R_i - R_o)(H + R_i + R_o)}}{2H}. \tag{2.14}$$

Here R_i and R_o are the radii of the inner and outer cylinders, respectively, and H is the center-to-center distance. The surface of the inner and outer cylinders are given by $\xi_1 = \sinh^{-1}(C/R_i)$ and $\xi_2 = \sinh^{-1}(C/R_o)$, respectively (refer to Fig. 2.3).

Assuming a steady, unidirectional flow in the $z-$direction, the Navier-Stokes equation reduces to

$$\nabla^2 u_z = \frac{1}{\mu} \frac{dp}{dz}. \tag{2.15}$$

We non-dimensionalize the velocity as $w = u_z/(GR_o^2/\mu)$, where G represents the magnitude of the pressure gradient in the $z-$direction. The dimensionless governing equation in bipolar cylindrical coordinate system is then given by

$$\frac{\partial^2 w}{\partial \xi^2} + \frac{\partial^2 w}{\partial \theta^2} = -\frac{C^2}{R_o^2(\cosh \xi - \cos \theta)^2}, \tag{2.16}$$

and the homogenous slip boundary conditions are given by

$$w = \pm \beta (\cosh \xi - \cos \theta) \frac{\partial w}{\partial \xi}\bigg|_{\xi = \xi_*}. \tag{2.17}$$

Here, $+$ is used when $\xi_* = \xi_1$ and $-$ is used when $\xi_* = \xi_2$. The slip coefficient β is related to slip length l as

$$\beta = \frac{l}{C}. \tag{2.18}$$

The solution of Eq 2.16 can be obtained as a superposition of a general solution to the Laplace equation and a particular solution accounting for the non-homogenous terms in Eq. 2.16 as

$$w = a_1 + a_2\xi + \sum_{n=1}^{\infty}[A_n \sinh(n(\xi-\xi_1)) + B_n \sinh(n(\xi-\xi_2))]\cos n\theta - \frac{C^2\cosh\xi}{2R_o^2(\cosh\xi - \cos\theta)}. \tag{2.19}$$

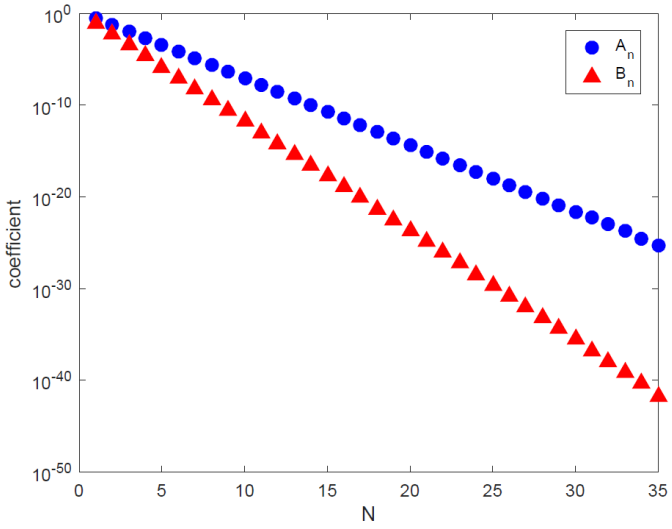

Figure 2.4: Coefficients A_n and B_n with number of terms N for slip length $(\lambda) = 0.1$.

The unknown coefficients in Eq. 2.19 are obtained by applying the boundary conditions and the orthogonality relations of the trigonometric functions as

$$\begin{aligned} &2a_1 + 2(\xi_* \mp \beta\cosh\xi_*)a_2 \pm \beta\cosh(\xi_* - \xi_1)A_1 \pm \beta\cosh(\xi_* - \xi_2)B_1 \\ &= \frac{C^2}{R_o^2}(\coth\xi_* \pm \beta(\cosh\xi_* - \sinh\xi_*)), \end{aligned} \tag{2.20}$$

$$\begin{aligned} &\pm 2\beta\delta_1 n a_2 \pm \beta(n-1)\cosh((n-1)(\xi_* - \xi_1))A_{n-1} \pm \beta(n+1)\cosh((n+1)(\xi_* - \xi_1))A_{n+1} \\ &+ (2\sinh(n(\xi_* - \xi_1)) - 2n(\pm\beta)\cosh\xi_*\cosh(n(\xi_* - \xi_1)))A_n \pm \beta(n-1)(\xi_* - \xi_2))B_{n-1} \\ &+ (2\sinh(n(\xi_* - \xi_2)) - 2n(\pm\beta)\cosh\xi_*\cosh(n(\xi_* - \xi_2)))B_n = \frac{C^2}{R_o^2}(2\coth\xi_* \\ &\pm 2\beta\cosh\xi_*)(\cosh\xi_* - \sinh\xi_*)^n, \end{aligned} \tag{2.21}$$

where n $\geq$ 1, δ_{ij} is the Kronecker delta and the signs $\pm$ are used as $+$ for $\xi_* = \xi_1$ and $-$ for $\xi_* = \xi_2$. Compared with previous results, we have corrected a typo in the

equation presented in Alassar [24]. With the assumptions that $\lim_{n\to\infty} A_n = 0$ and $\lim_{n\to\infty} B_n = 0$, the above system of equations can be solved for the required $2N+2$ coefficients by setting $A_N = B_N = 0$, where N is the number of terms considered in the series. The error involved is expected to be small when N is large. The coefficients A_n and B_n are computed (refer to Appendix for the MATLAB implementation) and shown in Fig. 2.4. As expected, the coefficients monotonically decrease and become very small as N increases.

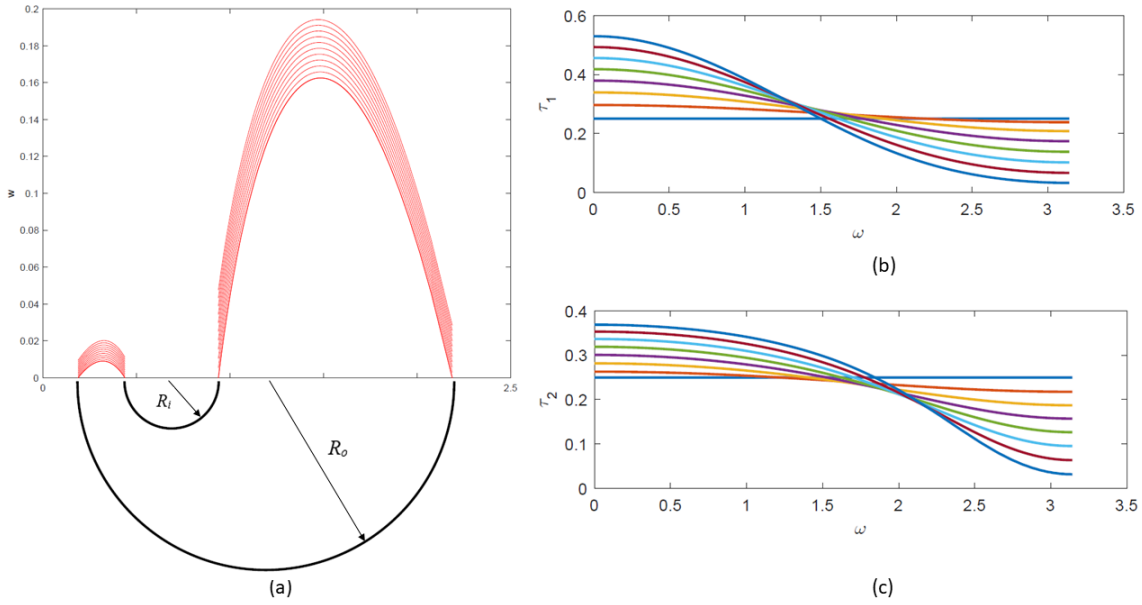

Figure 2.5: Results for homogeneous slip conditions (a) dimensionless velocity at $\theta = 0$ and π for $R_i/R_o = 1/4$ and $H/R_o = 1/2$, curves from top to bottom: $\beta =$ 0.1, 0.09, 0.08, 0.07, 0.06, 0.05, 0.04, 0.03, 0.02, 0.01 and 0.0. (b) dimensionless wall shear stress on inner cylinder (τ_1) for $\beta = 0.05$, $R_i/R_o = 1/2$ and eccentricity, $e =$ 0.001, 0.125, 0.250, 0.375, 0.5, 0.625, 0.750 and 0.875. (c) dimensionless wall shear stress on outer cylinder (τ_2) for $\beta = 0.05$, $R_i/R_o = 1/2$ and eccentricity, $e =$ 0.001, 0.125, 0.250, 0.375, 0.5, 0.625, 0.750 and 0.875.

The coefficients are then employed to compute the velocity field using Eq. 2.19 and shown in Fig. 2.5a. The results agree with those presented in Alassar [24] for various slip lengths. We also reproduce the results on wall shear stress, which is calculated

by

$$\tau = \mp \frac{\mu}{C}(\cosh\xi_* - \cos\theta)\frac{\partial u}{\partial \xi}\bigg|_{\xi=\xi_*}, \tag{2.22}$$

where the signs $\mp$ are used as $-$ when $\xi_* = \xi_1$ and $+$ when $\xi_* = \xi_2$. The reproduced results agree with those presented in Alassar [24] and are shown in Fig. 2.5(b) and (c) for inner and outer cylinders respectively for different eccentricity, $e = H/(R_o - R_i)$.

2.2.2 Non-homogenous slip

After reproducing the results for a homogenous slip in Alassar [24], we modify the boundary conditions (Eq. 2.17) for the problem in this study. The inner cylinder (pacemaker lead) at $\xi = \xi_1$ can be slippery while the outer cylinder at $\xi = \xi_2$ (blood vessel) has the no-slip boundary condition:

$$w(\xi = \xi_1) = \beta_1(\cosh\xi - \cos\theta)\frac{\partial w}{\partial \xi}\bigg|_{\xi=\xi_1} \quad \text{and} \quad w(\xi = \xi_2) = 0. \tag{2.23}$$

With non-homogeneous slip boundary conditions in Eq. 2.23, the system of equations given by Eqs. 2.20 and 2.21 are solved again with the modified values of $\beta = \beta_1$ at $\xi = \xi_1$ and $\beta = 0$ at $\xi = \xi_2$. The new coefficients A_n and B_n are shown in Fig. 2.6. The velocity field is then obtained using the new coefficients with Eq. 2.19.

For illustration, we consider a specific geometry defined by $R_o = 0.55$ cm, $R_i = 0.1167$ cm and $H = 0.144$ cm. We assume a viscosity of $\mu = 0.04$ g/cm.s and density $\rho = 1.06$ g/cm^3 for blood and a physiological volume flow rate $Q = 16$ cm^3/s. In Fig. 2.7b, the velocity profiles for different values of slip length λ are plotted along the line of centers shown as a bold black line in Fig. 2.7a. The slip velocity at the inner cylinder increases with the slip length, and a dimensionless slip length of $\lambda = 1$ is already effective in inducing a significant slip velocity compared with that with $\lambda = 10$.

The wall shear stress on the outer cylinder (representing the blood vessel) is also computed using Eq. 2.22 at $\xi = \xi_2$. Since the wall shear stress on the upper half of the vessel ($\omega \in [0, \pi]$, shown as the bold line in Fig. 2.8a) is the same as the lower half, we present only the results for the upper half of the vessel in Fig. 2.8b. Due to the eccentricity, the wall shear stress becomes non-uniform in general in contrast to the concentric case. For the case of no-slip ($\lambda = 0$), the wall shear stress is highly

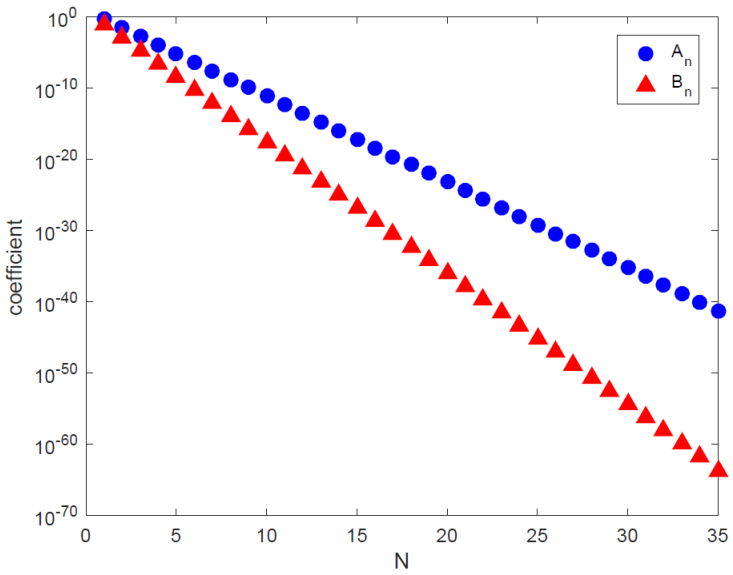

Figure 2.6: Coefficients A_n and B_n with number of terms N with non-homogenous slip lengths ($\lambda_1 = 0.1$ and $\lambda_2 = 0$).

non-uniform with a large peak at $\omega = 0$. With the increase in slip length (e.g. $\lambda = 1$ and 10), the wall shear-stress becomes more uniform and reduces to a level close to the case when there is no lead (compared with Fig. 2.2). These characteristics may be desirable from a physiological perspective since the presence of the lead does not significantly alter the biomechanical environments and hence may lead to fewer side effects or complications.

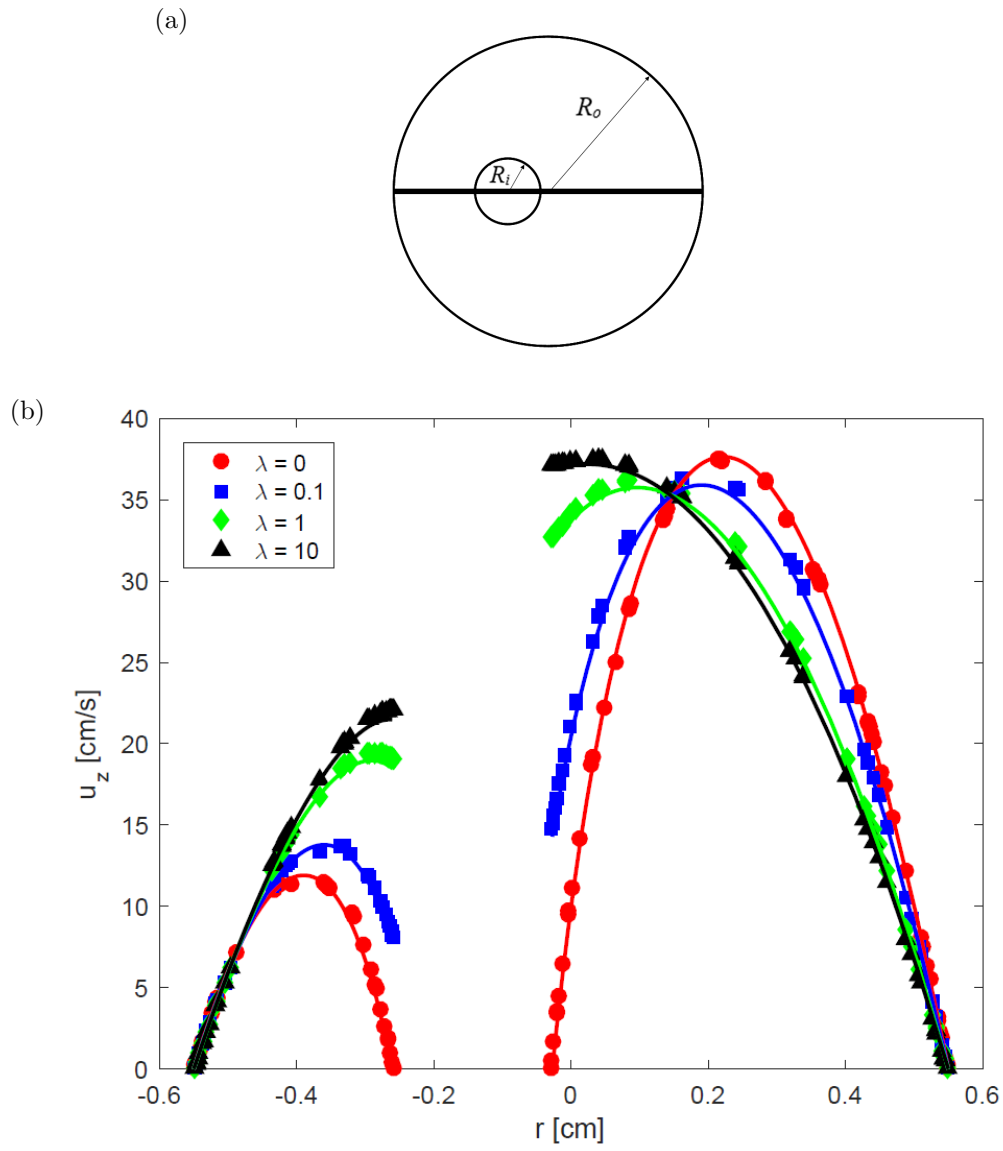

Figure 2.7: (a) Idealized eccentric model considered for the analytical and numerical studies. The bold black line along the line of centers represents the domain where the velocity distribution shown in (b) is plotted. (b) Comparison of velocity profiles along the line of centers for eccentric cylinders with a no-slip boundary condition at the outer cylinder and different dimensionless slip lengths $\lambda = 0$, 0.1, 1 and 10 at the inner cylinder. The solid lines represent analytical solution derived in this study and the symbols represent numerical results presented in Ch. 3.

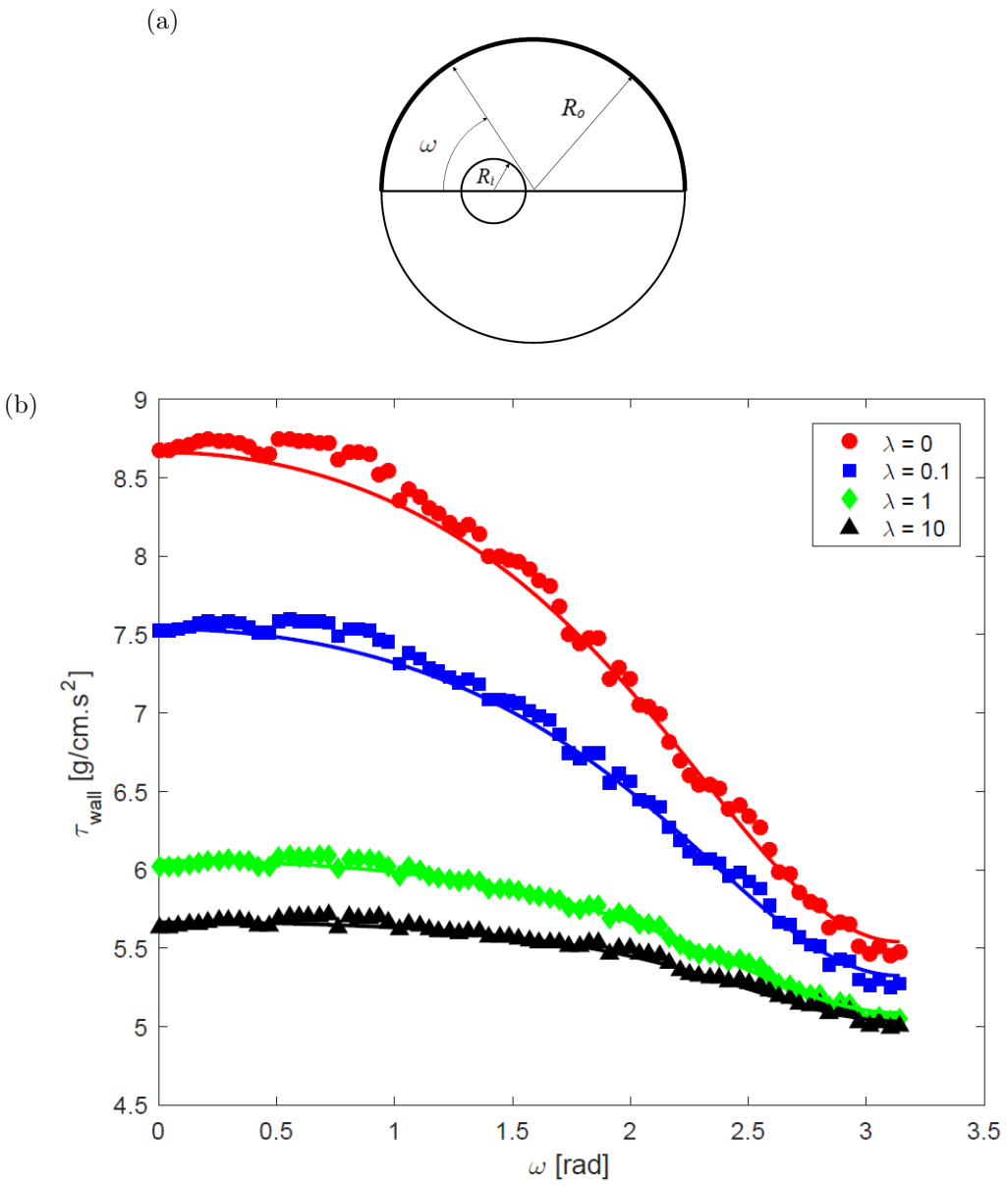

Figure 2.8: (a) Idealized eccentric model considered for the analytical and numerical studies. The bold black line represents the domain where the wall shear stress in (b) is plotted. (b) Comparison of wall shear stress on outer cylinder with no-slip boundary condition and inner cylinder with different dimensionless slip lengths $\lambda = 0$, 0.1, 1 and 10. The solid lines represent the analytical solution derived in this section and the symbols represent the numerical results presented in Ch. 3.

Chapter 3

Computational Results

3.1 Numerical implementation and validation

An open source software SimVascular [25] was employed to create models and simulate blood flow. Three dimensional incompressible Navier-Stokes equations were discretized by a stabilized finite element formulation (SUPG: streamlined upwind Petrov-Galerkin). A generalized alpha-method with second order accuracy in time is used for time integration [26]. Further details on the finite element solver can be found in [27–29].

The numerical simulations are first validated against the analytical results derived for idealized geometrical model studied in Ch. 2 in Sec. 3.1 before proceeding to consider more a geometrically complex patient-specific model in Sec. 3.2. The Dirichlet boundary condition was employed for the inlet with prescribed flow rates and a parabolic profile. The same flow rate ($Q = 16$ cm^3/sec) at the inlet and fluid properties (μ =0.04 g/cm.s and $\rho = 1.06$ g/cm^3) are prescribed as the analytical solutions. A resistance boundary condition was employed for the outlet [30]. A rigid-wall approximation was employed. No slip boundary condition was prescribed on the vessel wall, and a Navier slip boundary condition was enforced on the pacing lead to model the effect of a slippery surface.

Meshsim (Simmetrix, Clifton Park, NY) was used to generate linear tetrahedral meshes. The same geometrical models of concentric and eccentric cylinders considered in Ch. 2 are constructed for numerical simulations. The idealized model measures inner and outer radii of 0.1167 cm and 0.55 cm respectively with a length of 100

times of the outer diameter, and it consists of 6M elements with a mesh size of 0.08 cm. A three-layer boundary mesh with a factor of 0.5 is added to the wall. The mesh size was chosen such that the error between numerical and analytical results in terms of velocity and wall shear-stress distributions are less than 4%.

The numerical results are represented as symbols in the velocity plots for the concentric (Fig. 2.1) and eccentric (Fig. 2.7b) cases. Similarly, the wall shear stress obtained numerically are compared with the analytical solutions for the concentric (Fig. 2.2) and eccentric (Fig. 2.8b) cases. Satisfactory agreements between the numerical and analytical results with error less than 4% are obtained. Fig. 3.1, shows the change velocity distributions for concentric and eccentric geometries (with center-to-center distance $H = 0,\ 0.144,\ 0.289$ cm from left to right columns) for visualization of the effect of slip on the pacemaker lead on the overall flow field. The presence of a pacemaker lead in a blood vessel alters the flow characteristics compared with the case when there is no lead. The case of no-slip surface modifies the overall flow field significantly, and the introduction of a slippery surface ($\lambda = 1$) makes the alternation less apparent. A dimensionless slip length of $\lambda = 1$ already induces effects similar to that by the complete slip case $\lambda = \infty$.

3.2 Patient-specific model: no-slip vs. slippery surfaces

In this section, we investigate the effect of a slippery pacemaker lead surface in more complex geometries in an actual patient with a pacemaker installed. The medical images are obtained through collaboration with School of Medicine at Stanford University. A patient-specific model is created from the CT-scan images using SimVascular (Fig, 3.2). The patient specific model consists of 1.2 M elements. Then, this model is used to run simulations with no-slip and with slip conditions on the pacemaker lead surface. As mentioned in the Introduction, current technologies can create a slippery surface with slip length on the order of hundreds of micrometers [17]. Here we consider a slip length of $l = 800\ \mu$m to compare the effect of no-slip vs. slipper surfaces in a realistic physiological geometry.

Velocity distributions at various cross sections in the blood vessel are displayed in Fig. 3.3 to compare the no-slip and slipper cases. Similar to the idealized geometries,

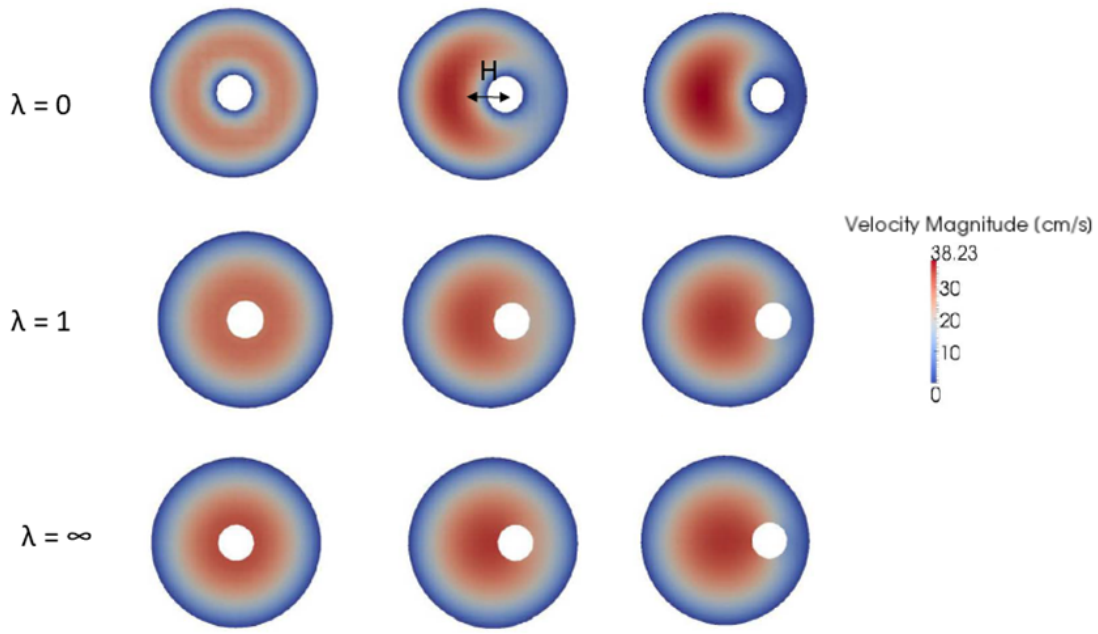

Figure 3.1: Velocity distributions for different eccentricities (from left to right columns: $H = 0$ cm, 0.144 cm and 0.289 cm) with different slip lengths ($\lambda = 0$, 1, ∞).

as expected the slippery surfaces reduce the region of flow stasis near the lead at various locations along the blood vessel. Since flow stasis has been associated with the risk of developing thrombosis, the reduction of such regions by the use of slippery surface may help reduce the risk of venous occlusions.

The wall shear stress distribution on the blood vessel is shown in Fig. 3.4 for the case without lead, with a no-slip lead, and with a slippery lead. Compared with the case where there is no lead (a), the wall shear stress when there is a no-slip lead is elevated (b). The presence of a slippery surface (c) helps bring the shear stress level closer to the case where there is no lead. This may reduce the possibility of any undesirable mechanobiological response of the endothelial cells along the blood vessel.

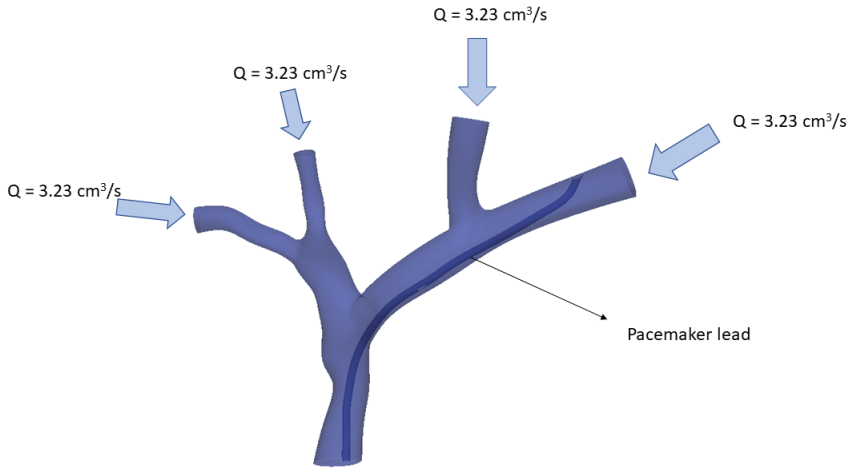

Figure 3.2: Patient model obtained from CT-scan. The arrows and numbers indicate the inlet volume flow rates of blood.

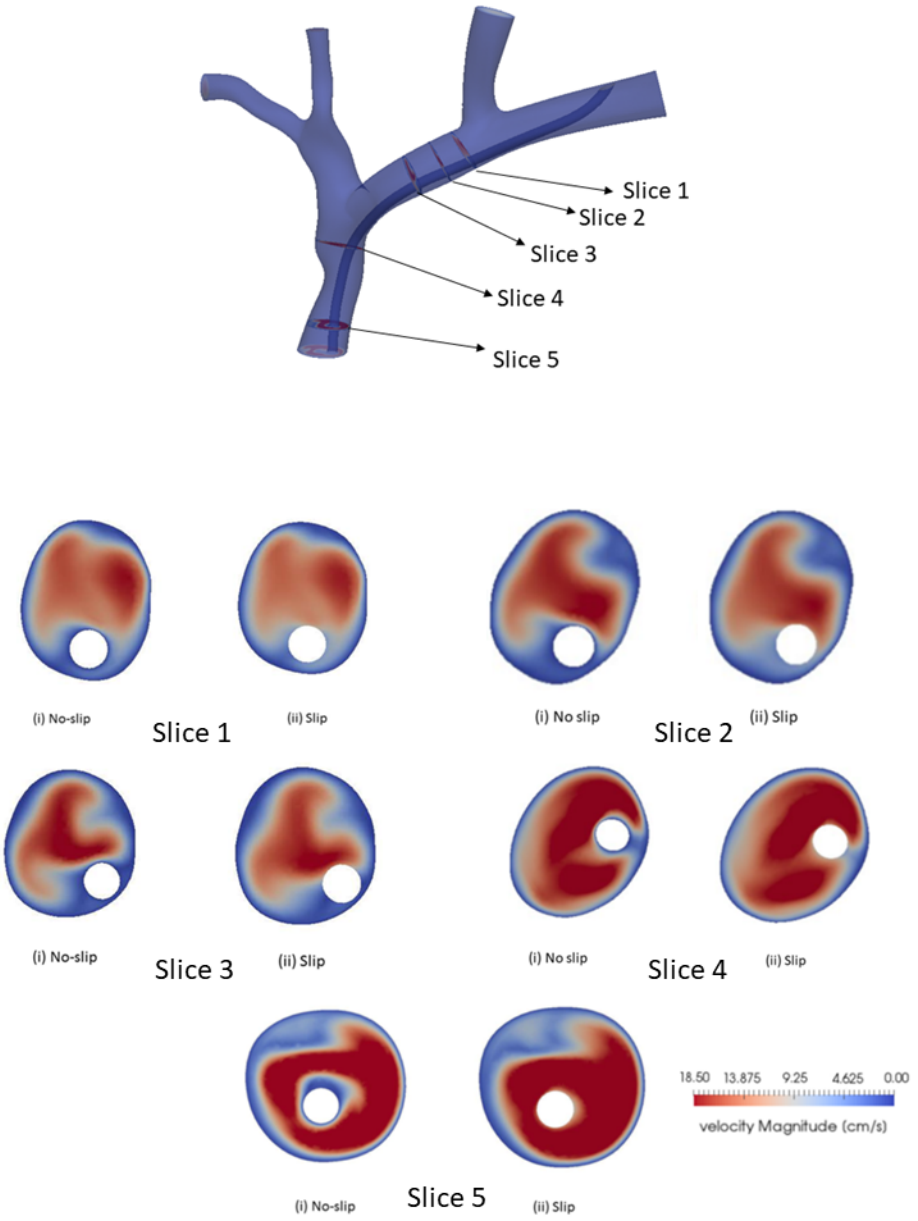

Figure 3.3: Visualization of the flow distribution at various cross sections along the blood vessel for the case when the pacemaker lead surface is no-slip and slippery.

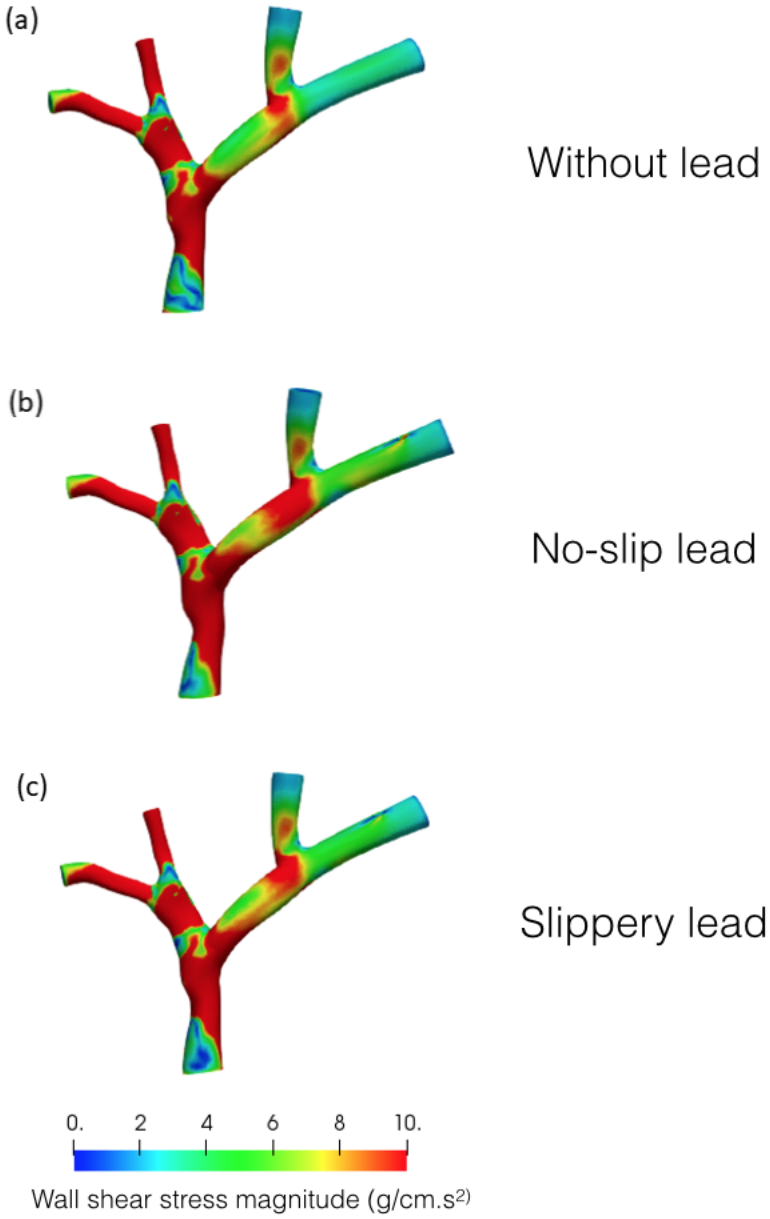

Figure 3.4: Wall shear stress distribution on the blood vessel, (a) without pacemaker lead, (b) with no-slip pacemaker lead ($l = 0$ μm) and (c)with slippery pacemaker lead ($l = 800$ μm).

Chapter 4

Conclusions

While treating a patient with arrhythmia, where the patient's heart does not beat properly, a pacemaker is implanted in the body to make heart beat normally. The presence of the lead in the blood vessel modifies the flow environment in the vessel. Regions of flow stasis have been suggested to increase the risk of venous occlusions in previous studies. In particular, these regions were identified in previous studies to be near the pacemaker leads. With recent technologies capable of creating slippery surfaces, we perform analytical and numerical studies how the flow structures can be modified by replacing no-slip pacemaker slips by these slippery surfaces.

The effect of a slippery surface is modeled through a Navier slip boundary condition. Analytical studies were first performed with idealized geometries including slip flow past an eccentric annulus with non-homogenous slip boundary conditions. The presence of a slippery surface increases the velocity around the pacemaker leads and help restore the wall shear stress at the blood vessel to a level closer to the case when there is no lead. These analytical results were employed to validate numerical simulations, which showed satisfactory agreements. A patient-specific model was then constructed to evaluate the influence of the slippery pacemaker lead surface in a more realistic physiological environment. Qualitatively similar behaviors were obtained in the patient-specific model. The use of slippery pacemaker leads instead of the conventional pacemaker lead may help reduce the risk of venous occlusions. However, more extensive case studies with realistic patient geometries and experimental investigations in the future are required to further examine this idea.

References

[1] Rozmus G., Daubert J. P., Huang D. T., Rosero S., Hall B., Francis C. "Venous Thrombosis and Stenosis After Implantation of Pacemakers and Defibrillators." Journal of Interventional Cardiac Electrophysiology, 13, 9-19, 2005.

[2] Korkeila P., Nyman K., Ylitalo A., Koistinem J., Karjalainen P., Lund J., Airaksinen K. E. J. "Venous Obstruction After Pacemaker Implantation." Pacing and Clinical Electrophysiology, 30, 199-206, 2007.

[3] Oginosawa Y., Abe H., Nakashima Y. "The Incidence and Risk Factors for Venous Obstruction After Implantation of Transvenous Pacing Leads." Pacing and Clinical Electrophysiology, 25, 1605-1611, 2002.

[4] Haghjoo M., Nikoo M. H., Fazelifar A. F., Alizadeh A., Emkanjoo Z., Sadr-Ameli M. A. "Predictors of venous obstruction following pacemaker or implantable cardioverter-defibrillator implantation: a contrast venographic study on 100 patients admitted for generator change, lead revision, or device upgrade." Europace, 9, 328-332, 2007.

[5] Sticherling C., Chough S. P., Baker R. L., Wasmer K., Oral H., Tada H., Horwood L., Kim M. H., Pelosi F., Michaud G. F., Strickberger S. A., Morady F., Knight B. P. "Prevalence of central venous occlusion in patients with chronic defibrillator leads." American Heart Journal, 141, 813-816, 2001.

[6] Lloyd-Jones D., Adams R. J., Brown T. M., Carnethon M., Dai S., Simone G. D., Ferguson T. B., Ford E., Furie K., Gillespie C., Go A., Greenlund K., Haase N., Hailpern S., Ho P. M., Howard V., Kissela B., Kittner S., Lackland D., Lisabeth L., Marelli A., McDermott M. M., Meigs J., Mozaffarian D., Mussolino M., Nichol G.,

Roger V. L., Rosamond W., Sacco R., Sorlie P., Stafford R., Thom T., Wasserthiel-Smoller S., Wong N. D., Wylie-Rosett J. "Heart Disease and Stroke Statistics - 2010 Update." Circulation, 121, 46-215, 2010.

[7] Figa F. H., McCrindle B. W., Bigras J. L., Hamilton R. M., Gow R. M."Risk factors for venous obstruction in children with transvenous pacing leads." Pacing Clin Electrophysiol, 20, 1902-1909, 1997.

[8] National Heart Lung and Blood Institute. How Does a Pacemaker works? Retrieved on: August 21, 2017: https://www.nhlbi.nih.gov/health/health-topics/topics/pace/howdoes

[9] Marsden A. L. "Optimization in Cardiovascular Modeling." Annual Review of Fluid Mechanics, 46, 519-546, 2014.

[10] Lonyai A., Dubin A. M., Feinstein J. A., Taylor C. A., Shadden S. C."New Insights into Pacemaker Lead-Induced Venous Occlusion: Simulation-Based Investigation of Alterations in Venous Biomechanics." Cardiovascular Engineering, 10, 84-90, 2010.

[11] Tuteja A., Choi W., Ma M., Mabry J. M., Mazzella S. A., Rutledge G. C., McKinley G. H., Cohen R. E."Designing Superoleophobic Surfaces." Science, 318, 1618-1622, 2007.

[12] Wong T.S., Kang S.H., Tang S.K.Y., Smythe E.J., Hatton B.D., Grinthal A., Aizenberg J. "Bioinspired self-repairing slippery surfaces with pressure-stable omniphobicity." Nature, 447, 443-447, 2011.

[13] Leslie D. C., Waterhouse A., Berthet J. B., Valentin T. M., Watters A. L., Jain A., Kim P., Hatton B. D, Nedder A., Donovan K., Super E. H., Howell C., Johnson C. P., Vu T. L., Bolgen D. E., Rifai S., Hansen A. R., Aizenberg M., Super M., Aizenberg J., Ingber D. E."A bioinspired omniphobic surface coating on medical devices prevents thrombosis and biofouling." Nature Biotechnology, 32, 1134-1140, 2014.

[14] Joseph P., Cottin-Bizonne C., Benoit J. M., Ybert C., Journet C., Tabeling P., Bocquet L. "Slippage of water past superhydrophobic carbon nanotube forests in microchannels." Physical Review Letters, 97, 156104, 2006.

[15] Choi C. H., Kim C. J."Large slip of aqueous liquid flow over a nanoengineered superhydrophobic surface." Physical Review Letters, 96, 066001, 2006.

[16] Srinivasan S., Choi W., Park K. C., Chhatre S. S., Cohen R. E., McKinley G. H."Drag reduction for viscous laminar flow on spray-coated non-wetting surfaces." Soft Matter, 9, 5691-5702, 2013.

[17] Solomon B. R., Khalil K. S., Varanasi K. K. "Drag Reduction using Lubricant-Impregnated Surfaces in Viscous Laminar Flow." Langmuir, 30, 10970-10976, 2014.

[18] Brenner M. P., Stone H. A. "Microfluidics: The No-Slip Boundary Condition." Chapter 19 in: Handbook of Experimental Fluid Dynamics, C. Tropea, A. Yarin, J. F. Foss (Eds.), Springer, Ch. 19, 1219-1240, 2007.

[19] Wang C.Y. "Brief Review of Exact Solutions For Slip-Flow in Ducts and Channels." Journal of Fluids Engineering, 134, 094501, 2012.

[20] Bar-Cohen Y., Berul C. I., Alexander M. E., Fortescue E. B., Walsh E. P., Triedman J. K., Cecchin F. "Age, Size, and Lead Factors Alone Do Not Predict Venous Obstruction in Children and Young Adults with Transvenous Lead Systems." Journal of Cardiovascular Electrophysiology, 17, 754-759, 2006.

[21] Taylor C. A., Draney M. T., Ku J. P., Parker D., Steele B. N., Wang K., Zarins C. K. "Predictive Medicine: Computational Techniques in Therapeutic Decision-Making." Computer Aided Surgery, 4, 231-247, 1999.

[22] Wilson N., Wang K., Dutton R. W., Taylor C. "A Software Framework for Creating Patient Specific Geometric Models from Medical Imaging Data for Simulation Based Medical Planning of Vascular Surgery." Medical Image Computing and Computer-Assisted Intervention – MICCAI, 449-456, 2001.

[23] Wilson N. M., Arko F. R., Taylor C. A. "Predicting changes in blood flow in patient-specific operative plans for treating aortoiliac occlusive disease." Computer Aided Surgery, 10, 257-277, 2005.

[24] Alassar R. S. "Slip Flow in Eccentric Annuli." Journal of Fluids Engineering, 139, 041201, 2017.

[25] Updegrove A., Wilson N. M., Merkow J., Lan H., Marsden A. L., Shadden S. C. "Simvascular: An open source pipeline for cardiovascular simulation." Annals of biomedical engineering, 45, 525-541, 2017.

[26] Jansen K. E., Whiting C. H., Hulbert G. M. "A generalized-α method for integrating the filtered Navier–Stokes equations with a stabilized finite element method." Computer methods in applied mechanics and engineering, 190, 305-319, 2000.

[27] Brooks A. N., Hughes T. J. R. "Streamline upwind/Petrov-Galerkin formulations for convection dominated flows with particular emphasis on the incompressible Navier-Stokes equations." Computer methods in applied mechanics and engineering, 32, 199-259, 1982.

[28] Taylor C. A., Hughes T. J. R., Zarins C. K. "Finite element modeling of blood flow in arteries." Computer methods in applied mechanics and engineering, 158, 155-196, 1998.

[29] Whiting C. H., Jansen K. E. "A stabilized finite element method for the incompressible Navier-Stokes equations using a hierarchical basis." International Journal for Numerical Methods in Fluids, 35, 93-116, 2001.

[30] Vignon-Clementel I. E., Figueroa C. A., Jansen K. E., Taylor C. A. "Outflow boundary conditions for three-dimensional finite element modeling of blood flow and pressure in arteries." Computer methods in applied mechanics and engineering, 195, 3776-3796, 2006.

[31] Behr M. "On the application of slip boundary condition on curved boundaries," International journal for numerical methods in fluids, 45, 43-51, 2004.

[32] SimVascular (http://simvascular.github.io/)

Appendix A

MATLAB Code

Coefficient code

```
clear all
hr2 = 1/2;
r1r2 = 1/4;
cr2 = sqrt((hr2 r1r2  1)*(hr2 r1r2+1)*(hr2+r1r2 1)*(hr2+r1r2
    +1))/(2*hr2);
xi1 = asinh(cr2/r1r2);
xi2 = asinh(cr2);
beta = 0.1;
% change i for different number of terms
i =35 ;
s = i+1;
xi = xi1;
A = sym('A',[1 i]);
B = sym('B',[1 i]);
syms a1 a2
beta1 = beta;
eqnG(1) = 2*a1+a2*2*(xi+beta1*cosh(xi)) A(1)*(beta1*cosh(xi
    xi1))   B(1)*(beta1*cosh(xi xi2))== (cr2^2)*(coth(xi)
    beta1*(cosh(xi) sinh(xi)));
for n = 1:i
    if n==1
```

```
19      eqnG(n+1) = 2*beta1*a2  beta1*(n+1)*cosh((n+1)*(xi  xi1))
           *A(n+1) + (2*sinh(n*(xi  xi1))+2*n*beta1*cosh(xi)*cosh(
           n*(xi  xi1)))*A(n)    beta1*(n+1)*cosh((n+1)*(xi  xi2))*B
           (n+1) + (2*sinh(n*(xi  xi2))+2*n*beta1*cosh(xi)*cosh(n
           *(xi  xi2)))*B(n) == cr2^2*((cosh(xi)  sinh(xi))^n)*(2*
           coth(xi) 2*beta1*cosh(xi));
20      else if n==i
21           eqnG(n+1) =  beta1*(n 1)*cosh((n 1)*(xi  xi1))*A(n
                1) + (2*sinh(n*(xi  xi1))+2*n*beta1*cosh(xi)*
                cosh(n*(xi  xi1)))*A(n)  beta1*(n 1)*cosh((n 1)*(
                xi  xi2))*B(n 1) +(2*sinh(n*(xi  xi2))+2*n*beta1*
                cosh(xi)*cosh(n*(xi  xi2)))*B(n) == cr2^2*((cosh(
                xi)  sinh(xi))^n)*(2*coth(xi) 2*beta1*cosh(xi));
22         else
23      eqnG(n+1) =  beta1*(n 1)*cosh((n 1)*(xi  xi1))*A(n 1)
           beta1*(n+1)*cosh((n+1)*(xi  xi1))*A(n+1) + (2*sinh(n*(
           xi  xi1))+2*n*beta1*cosh(xi)*cosh(n*(xi  xi1)))*A(n)
           beta1*(n 1)*cosh((n 1)*(xi  xi2))*B(n 1)  beta1*(n+1)*
           cosh((n+1)*(xi  xi2))*B(n+1)+(2*sinh(n*(xi  xi2))+2*n*
           beta1*cosh(xi)*cosh(n*(xi  xi2)))*B(n) == cr2^2*((cosh(
           xi)  sinh(xi))^n)*(2*coth(xi) 2*beta1*cosh(xi));
24         end
25      end
26 end
27 xi = xi2;
28 t = s+1;
29 beta2 =  beta;
30 eqnG(t) =  2*a1+a2*2*(xi+beta2*cosh(xi)) A(1)*(beta2*cosh(xi
      xi1))  B(1)*(beta2*cosh(xi  xi2))== (cr2^2)*(coth(xi)
      beta2*(cosh(xi)  sinh(xi)));
31 for n = 1:i
32      t = t+1;
33      N(i) = i;
```

```
34        if n==1
35           eqnG(t) = 2*beta2*a2  beta2*(n+1)*cosh((n+1)*(xi xi1
                ))*A(n+1) + (2*sinh(n*(xi xi1))+2*n*beta2*cosh(xi)
                *cosh(n*(xi xi1)))*A(n)  beta2*(n+1)*cosh((n+1)*(
                xi xi2))*B(n+1) + (2*sinh(n*(xi xi2))+2*n*beta2*
                cosh(xi)*cosh(n*(xi xi2)))*B(n) == cr2^2*((cosh(xi
                ) sinh(xi))^n)*(2*coth(xi) 2*beta2*cosh(xi));
36         else if n==i
37                   eqnG(t) = beta2*(n 1)*cosh((n 1)*(xi xi1))*
                        A(n 1) + (2*sinh(n*(xi xi1))+2*n*beta2*
                        cosh(xi)*cosh(n*(xi xi1)))*A(n) beta2*(n
                         1)*cosh((n 1)*(xi xi2))*B(n 1) +(2*sinh(
                        n*(xi xi2))+2*n*beta2*cosh(xi)*cosh(n*(xi
                         xi2)))*B(n) == cr2^2*((cosh(xi) sinh(xi)
                        )^n)*(2*coth(xi) 2*beta2*cosh(xi));
38              else
39           eqnG(t) = beta2*(n 1)*cosh((n 1)*(xi xi1))*A(n 1)
                beta2*(n+1)*cosh((n+1)*(xi xi1))*A(n+1) + (2*sinh(
                n*(xi xi1))+2*n*beta2*cosh(xi)*cosh(n*(xi xi1)))*A
                (n) beta2*(n 1)*cosh((n 1)*(xi xi2))*B(n 1)
                beta2*(n+1)*cosh((n+1)*(xi xi2))*B(n+1)+(2*sinh(n
                *(xi xi2))+2*n*beta2*cosh(xi)*cosh(n*(xi xi2)))*B(
                n) == cr2^2*((cosh(xi) sinh(xi))^n)*(2*coth(xi) 2*
                beta2*cosh(xi));
40              end
41        end
42  end
43
44  [C,D] = equationsToMatrix([eqnG],[a1,a2,A,B]);
45  X = linsolve(C,D);
46  double(X);
47  double(C);
48  An(1:i) = double(X(3:i+2));
```

```
Bn(1:i) = double(X(3+i:2*i+2));
An;
Bn;
semilogy(abs(An),' bo','LineWidth',2,'MarkerFaceColor','b');
    hold on;
semilogy(abs(Bn),' r^','LineWidth',2,'MarkerFaceColor','r');
    hold off; legend('A_n','B_n');
```

Velocity code

```
theta = 0;
syms abc
w =0;
cde = 0;
a = X(1);
b = X(2);
for n = 1:i
    cde = cde + (An(n)*sinh(n*(abc xi1))+Bn(n)*sinh(n*(abc
        xi2)))*cos(n*theta);
end
w =  c^2*cosh(abc)/(2*(cosh(abc) cos(theta))) + X(1) + X(2)*
    abc + cde;
x1 = c*sinh(abc)/(cosh(abc) cos(theta));
fplot(x1,w, [xi2 xi1], 'r'); hold on;

theta = pi;
syms abc
w1 =0;
cde = 0;
a = X(1);
b = X(2);
for n = 1:i
    cde = cde + (An(n)*sinh(n*(abc xi1))+Bn(n)*sinh(n*(abc
        xi2)))*cos(n*theta);
end
```

```
w1 =  c^2*cosh(abc)/(2*(cosh(abc) cos(theta))) + X(1) + X(2)*
    abc + cde;
x2 = c*sinh(abc)/(cosh(abc) cos(theta));
fplot(x2,w1, [xi2 xi1], 'k'); hold on;
legend('\theta = 0', '\theta = pi')
xlim([0  2.5]);
ylim([0  0.26]);
```

Wall shear stress code

```
abc = 0;
xi = xi;
mn = 1000;
theta1 = linspace(0,pi,mn);
for n = 1:i
    abc =  abc+ (An(n)*n*cosh(n*(xi  xi1))+Bn(n)*n*cosh(n*(xi
        xi2)))*cos(n.*theta1);

end
dw1 =  c^2.*( cos(theta1)*sinh(xi))./(2*(cosh(xi) cos(theta1)
    ).^2) + X(2) + abc;
t1 = dw1.*(cosh(xi) cos(theta1))/c;

xy = c*sinh(xi)./(cosh(xi) cos(theta1));
yz = c.*sin(theta1)./(cosh(xi) cos(theta1));
x01 = c*coth(xi);
w1 = atan(yz./(xy x01));
op = 0;
for m = 2:mn
    op = op+1;
    if (w1(m 1) > w1(m))
        break
        %w1(m) = w1(m) + pi;
    end
end
```

```
24 w1(op+1:mn) = w1(op+1:mn) + pi;
25
26 plot(w1,t1,'Linewidth',1.5); hold on;
27 pbaspect([3 1 1])
28 ylim([0 0.4])
29 xlabel('w')
30 ylabel('\tau_2')
```